Mapping and evaluation of burned land from multitemporal analysis of AVHRR NDVI images

M. Pilar Martín and E. Chuvieco

Departamento de Geografía, Universidad de Alcalá de Henares, Colegios, 2
28801 Alcalá de Henares (Spain). Tel.: 341 8854438, Fax: 341 8854439

ABSTRACT

Several studies have addressed the application of NOAA-AVHRR channel 3 data to fire detection and mapping. However, its low thermal sensitivity and high signal to noise ratio make operational use of these data very complex. This paper explores multitemporal analysis of Vegetation Indexes as an alternative method for mapping and evaluation of large forest fires. Examples are presented for fires affecting the Mediterranean coast of Spain in the summer of 1991. Multitemporal registration of HRPT (High Resolution Picture Transmission) images was performed using both orbital and ground control point information. Change detection techniques were applied to discriminate burned land on single scenes, as well as on maximum value composites (MVC). Accuracy was tested using fire reports and a set of Landsat-TM images for the largest fire. Agreement between our estimations and the statistics provided by the Spanish forest service were up to 97 % for large fires using single images and 94 % using MVC.

1. INTRODUCTION

Fire detection and mapping from remote sensors has been generally performed on middle infrared bands because they are more sensitive to high temperature sources (Robinson, 1991). Forest fires with a flame temperature of 900 K have emittances 5,153 greater than average land cover in the middle infrared band (3.75 μm). This radiative contrast is much less clear in the thermal band (11.9 μm), where forest fires of that temperature would have only 38 times more emittance than healthy vegetation (Milne and Hall, 1992).

Experiences in using middle infrared sensors for fire detection and mapping include airborne scanners (Hirsch *et al.*, 1971; Matthews and Jessel, 1992), as well as satellite systems (e.g. Chuvieco and Martín, 1994a).

Most of the studies of forest fire mapping from AVHRR images rely on the sensitivity of channel 3 data for detecting fire events (e.g. Chuvieco and Martín, 1994a). In other words, the burned area is estimated from the active fires as detected by the middle infrared band. Usually, the total burned area is obtained from extrapolation of that burning area over a period of time, considering average fire duration (Setzer and Pereira, 1991b).

This method requires a fire to be active when the image is acquired. It also assumes that channel 3 data have a good accuracy for discriminating burning spots. Both requirements are often not fulfilled. Firstly, the frequency of AVHRR acquisitions can be reduced by cloud coverage or gaps in reception, making daily coverage unreliable. Secondly, the thermal sensitivity of channel 3 is rather poor, as the sensor is saturated at 320 K, and includes a high level of noise (Robinson, 1991). In the case of Mediterranean forest, fire spots can be easily confused with agricultural burns or even with bare soils, which frequently reach the saturation temperature in the summer during the afternoon pass (Belward, 1991). Discrimination from agricultural fires could be partially achieved by choosing evening or night images, because this type of burning tends to be done during daylight periods (Malingreau, 1990). Fire active areas and bare soils are also discernible on night images, as a result of the lower soil temperatures at this time (Langaas, 1992).

On the other hand, low thermal sensitivity of AVHRR channel 3 data may also create problems of overestimation of the burned area. It should be noted that a pixel may be saturated even if only a small proportion is actually occupied by fire. In fact, fires with a temperature above 500 K, even if they occupy less than 0.1 % of the pixel size, will most likely reach pixel saturation temperatures (Kaufman

et al., 1990). For this reason, a consistent tendency of overestimation has been found when AVHRR channel 3 fire mapping estimations are compared with higher resolution data, such as Landsat-MSS or TM. According to several experiences in the Amazon basin, this overestimation is in the order of 43 % (Setzer and Pereira, 1991a), or 1.5 times the areal extent observed with Landsat-TM (Pereira *et al.*, 1991).

In spite of these problems, the use of AVHRR channel 3 data for fire detection and mapping has been successfully tested in several studies. High accuracy for detecting large-scale forest fires was found in a pilot study conducted in Alberta. Overall, 46 percent of the total number of fires were located with data obtained from AVHRR channel 3. This accuracy increased to 80 % when only fires in cloud-free images were considered. Precision reached 95 %, when only medium to large fires (over 40 hectares) were taken into account. Accuracy for small fires was limited, 10 to 12 %, although better results were reported if only cloud-free areas were considered (up to 87 %; Flannigan and Vonder Haar, 1986). In the Brazilian Amazonia, analysis of AVHRR channel 3 images for the summer season of 1987 yielded a total estimation of 350,000 fires, covering as much as 200,000 sq km (Setzer and Pereira, 1991b). These results were obtained from the extrapolation of observed fires in 46 AVHRR images acquired from July to October. Pixels with high temperatures in channel 3 were labelled as fires and these calculations were extrapolated to cover the whole study period based on the average duration of fires and their average size. Channel 3 images have also been used to monitor fire growth in the case of large events (Chuvieco and Martín, 1994b).

In addition to the use of AVHRR imagery for fire detection and mapping, other sensors have also been shown to be useful. These studies include the use of geostationary data (Prins and Menzel, 1992), space photography (Herfert and Lulla, 1990), and DMSP *(Defense Meteorological Satellite Program)* night images (Cahoon *et al.*, 1992). Smoke emissions have also been monitored from the MAPS *(Measurement of Air Pollution from Satellites)* experiment on board the Space Shuttle (Watson *et al.*, 1990).

2. OBJECTIVES

As previously stated, most of the fire mapping projects using AVHRR images have been based on channel 3 data. We attempt to solve some of the problems reported with the use of this channel by the multitemporal analysis of NDVI (Normalized Difference Vegetation Index) images. Our approach is based on measuring the consequences of the fire, rather than detecting the fire itself.

Several studies have shown that spectral characteristics of burned land sharply contrast with the response of healthy vegetation. Burned land shows a severe decrease in near infrared reflectance, as a consequence of leaf deterioration, and an increase in red reflectance because of the lack of pigment absorption (Tanaka *et al.*, 1983; Chuvieco and Congalton, 1988). Therefore, the NDVI values of burned vegetation are much lower than for healthy plants, and multitemporal analysis should clearly portray the impact of fire. Some studies have proven this hypothesis, but using low spatial resolution data i.e. GAC (Global Area Coverage; Malingreau, 1984).

A secondary objective was to test the performance of single NDVI versus maximum value composites (MVC). As is well known, MVC is a standard procedure to reduce the effects of atmospheric and view-angle disturbances of AVHRR data (Holben, 1986). However, precise registration of single images is required to map fire perimeter, otherwise, mis-registration may make it difficult to locate the borders of the burned land. As a consequence, MVC might underestimate the affected area, by blurring the contrast between healthy and scorched vegetation. In a recent study conducted on the boreal forest of Alaska, MVC images were successfully used for detecting the number of fires, especially larger ones (89.5 % for fires over 2,000 hectares), but they underestimated burned land (60 % of the area reported by the Forest Service in the case of fires over 2,000 hectares: Kasische *et al.*, 1993).

3. METHODS

3.1. Study area

The previous objectives were pursued by analyzing a large forest fire, referred to as Buñols Fire, occurring on the Mediterranean coast of Spain **(figure 1)** during the summer of 1991. This was one of the largest fires in Spain within the last decade. It affected more than 18,000 hectares of forest and shrub land.

The study area presents the typical characteristics of Mediterranean coastal mountains covered mainly by **Pinus Halepensis** and various types of shrubs. Elevation ranges from 0 to 1,200 meters and the topography is steep. Weather is influenced by the Mediterranean sea. Episodic and very intense storms are common during the Fall which is

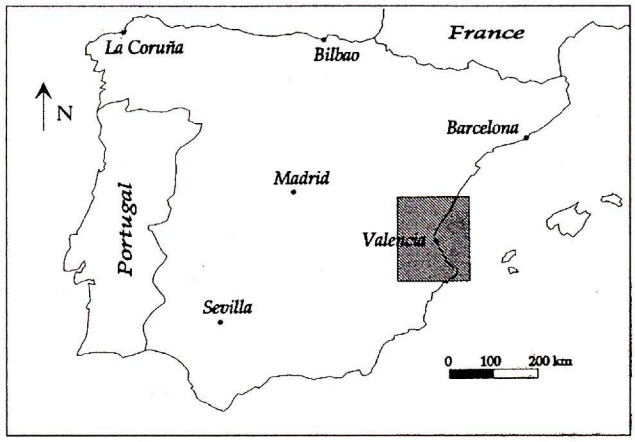

Figure 1 - Location of the study area

preceded by severe drought during the Summer season. Fire danger is closely related to wind velocity and direction. The highest incidence is associated with the western winds (continental and very dry). Human activities are considered extremely important in terms of fire danger for this area, because it is an important focus for tourism and also because the agricultural land use of the area. In other words, the threat of fire ignition can either originate from human or natural causes.

Buñol's fire was ignited by lightning on the afternoon of July 28. Two other human caused fires begun on July 30 (to the Southwest of the original nucleus), and on July 31 (to the North). Intense dry winds fuelled the spread of the fire which lasted until August 4. Within the area covered by the NOAA-AVHRR images, several other fires could be identified within the study period, also as a consequence of the intense drought and strong continental winds.

3.2. Image acquisition and correction

In order to have enough data on the environmental conditions from before and after the fire, all available HRPT (High Resolution Picture Transmission) images from July 10 to August 10 were acquired from the Maspalomas receiving station. Only NOAA-11 images were selected in order to maintain coherent processing conditions throughout the series. Unfortunately, during these days cloud coverage was unusually high, and as a result some images were not suitable for analysis. Moreover, there was a gap in the ESA archives between July 31 and the first days of August.

Geometrical correction of AVHRR images was performed in two steps. Firstly, an elliptical orbital model (originally developed by the Joint Research Center in Ispra and now included in the AVHRR-ERDAS module) was used. This program uses the Earth Location Points (ELP) included on the tape to adjust the correction, by assigning Mercator or Lambert projections to resampling. The Mercator projection was selected to properly adjust the resulting images to the Spanish UTM standard cartography. Secondly, image-to-image correction was carried out in order to reduce mis-

registrations between images. A set of 5 to 7 control points were selected to perform this adjustment. Considering the coarse pixel size of the AVHRR images only the main geographical features could be selected, such as dams, cities, specific vegetation patterns and major river crossings. Fitted equations were all linear because only minor adjustments between images were required. Estimated errors for the second correction were all less than 1 km. The final projection resembled the UTM standard cartography. As the images exceeded the size of a single UTM zone, we extended the central zone (30) to the East in order to maintain the pixel size throughout the image.

3.3. Generation of NDVI and MVC images

AVHRR images were ordered in raw format in order to speed up the delivery process. Therefore, the DN values had to be converted to reflectance for computing the NDVI. As NDVI is a ratio between the infrared and red reflectance, we eliminated all the constant terms of reflectance calculations (such as K, π and the cosine of the zenith angle), because they are invariant in the two bands. As a result, the final calculation of NDVI was done using albedos (Che and Price, 1992):

$$NDVI = \frac{L_2/S_2 - L_1/S_1}{L_2/S_2 + L_1/S_1} \quad (1)$$

where L_2 and L_1 are the radiances of AVHRR channels 2 and 1 (near infrared and red, respectively), and S_2 and S_1 are solar irradiances at the top of the atmosphere in those wavelengths. Conversion from the original digital values to radiance was done using the calibration coefficients provided by NOAA, which are also included in the ESA-SHARP format (ESA, 1992):

$$L_i = \alpha_i * (DN_i - Of_i) \quad (2)$$

where L_i is the radiance for band i; α_i is the calibration coefficient for band i; DN_i, the digital value recorded in

the image for that band, and Of_i, the deep space. For NOAA-11, $\alpha_1 = 0.612$, $\alpha_2 = 0.411$ (considering a monthly degradation rate after the launching: Che and Price, 1992), Of_1 and $Of_2 = 40$ (Holben *et al.*, 1990), $S_1 = 518.5$ and $S_2 = 335.2$ (Abel, 1990). Offsets and solar irradiance values are the ones used by the ESA in the SHARP-2 format (ESA, 1992).

As it is well known, NDVI values ranges from -1 to +1. Values greater than 0.2 refer to green vegetation. In order to stretch the results to an eight bit range, NDVI values were scaled using the following formula:

$$NDVI' = (NDVI + 1) * 125 \quad (3)$$

Maximum NDVI composites were generated for seven day periods. Considering the cloudy conditions on some days during the time series, an average number of four images were used to generate each MVC image.

3.4. Techniques for burned land mapping

Spatial and temporal profiles were obtained from the daily NDVI and MVC images to study the decrease in NDVI values caused by the fire (**figures 2 and 3**). We measured reductions of 0.2 to 0.4 in NDVIs for the areas most affected by the fire. It should be pointed out that this spectral contrast is gradually faded with vegetation recovery after the fire, so burned land evaluation should be done with images acquired as close as possible to the fire extinction date.

In this study, simple change detection techniques were used to discriminate the burned area. A pixel by pixel difference of both single NDVI and MVC values was calculated. We selected the best NDVI images (near to nadir and cloud free) from before and after the fire in order to perform discrimination on the daily scenes. For the MVC, the first (July 10 to 17) and the last (August 4 to 13) composites of the study series were selected.

To apply multitemporal differencing of NDVI values for fire mapping, it is critical to avoid cloud contamination, otherwise higher multitemporal decreases in NDVI might be related to cloud cover instead of to actual vegetation change. Cloud masking was accomplished using a ratio of the radiances in channels 1 and 4. Clouds present high radiances in the visible band and very low radiances in the thermal channels, so the highest ratio values can most probably be labelled as clouds. By visual screening, an interval of ratio values was got as a threshold in every image, and pixels within that range were set to 0, and the

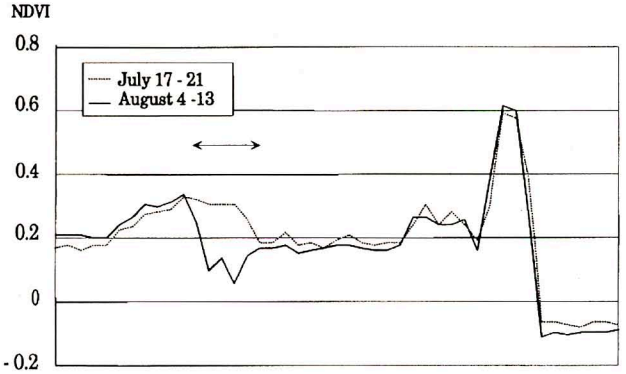

Figure 2 - Spatial profiles of NDVI values over the study area. The dotted line refers to values before the fire. The continuous line is taken from à MVC image after the fire

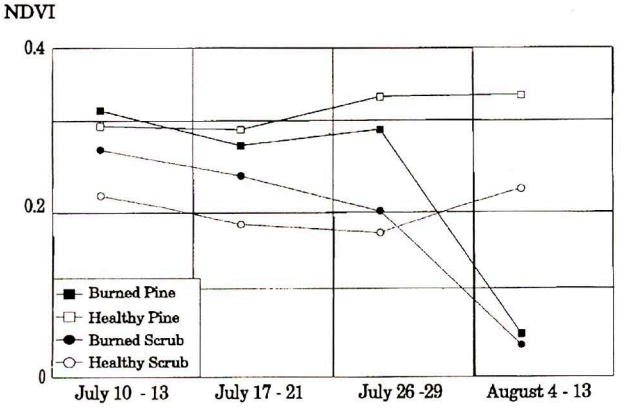

Figure 3 - Temporal evolution of NDVI values for burned and healthy pine and scrub land

remainder to 1. This cloud mask was multiplied by the individual NDVI scenes for generating cloud free NDVI images.

Afterwards, those areas with decreases in NDVI greater than 0.2 were classified as burned land, in both MVC and single day images. Those pixels were set to 1, while areas with lower decreases were assigned a value of 0. During the study period, several fires besides Buñol's affected the area included in the AVHRR window selected for this project. As a consequence, to compare results of our discrimination with official fire statistics, each fire had to be labelled with a different number. In order to do this, contiguous areas of pixels classified as burned land were grouped into unique categories using GIS clumping techniques. In other words, each fire (as defined by a group of contiguous burned pixels) was labelled with a specific number. A simple histogram of this clumped image made area estimation for each individual fire possible. **Figure 4** presents the final estimation of burned land using MVC and single NDVI values. The same number of fires were identified with both procedures. Although so far we have

considered Buñol's fire as a single event, in fact the area was affected by two different foci (Chiva, A, and Yatova, B), which were at the end of the fire, only separated by highway N-III, joining Madrid and Valencia. The other fires in the study region affected a much smaller area.

3.5. Accuracy assessment

Accuracy assessment was performed using both burned land statistics from fire reports and fire perimeters collected by GPS techniques. Fire reports are routinely generated by the Spanish Forest Service (ICONA). They generally include an estimation of burned land, as well as the species affected, but no information about the perimeter is provided. In the case of the Buñol's fire, a more detailed study was carried out, and the burned land perimeter was available on 1:50,000 scale maps. For the other fires affecting the study area, accuracy was only assessed using official statistics.

It should be pointed out that official statistics may also include some errors, as they are generally based on rough field estimations of burned land. Therefore, a more precise comparison can be obtained from cross analysis of AVHRR NDVI and higher resolution data, such as Landsat-TM imagery. Two Landsat-TM scenes from before and after the fire were acquired. After registration of both images, NDVI values were generated and burned area maps were obtained using the same change detection technique previously described. Unfortunately, the first available image after the fire was partially covered by clouds in the Eastern part of the burned perimeter. Consequently, we applied a cloud masking process to avoid errors in area estimation. This cloud mask was also applied to the AVHRR images in order to obtain a more precise assessment. For overlaying TM and AVHRR images, the latter was resampled to 30 x 30 meters.

4. RESULTS

4.1. Fire statistics

Table 1 presents the final estimation of burned land using MVC and single NDVI values. In Buñol's fire, burned land estimation with NDVI data is very close to the area measured by ICONA. The other fires in the study region affected a much smaller area, so we have grouped them into four clusters. There were some problems in identifying the specific fires in the official statistics of ICONA as fires affecting several municipalities are identified by the one in which the fire started. That is the case of the Carcagente fire (D+E), where disagreement between fire estimation and fire statistics is very high, most probably as a result of inappropriate identification of fire reports. As a matter of fact, fire report from fire authorities of the Autonomous region of Valencia estimated burned area in this fire to be 2,550 hectares. Excluding this problem, agreement between satellite estimation and fire statistics is within ± 15 % for most fires.

Table 1 - Area evaluation of burned land according to ICONA's reports and NDVI multitemporal analysis (in hectares)

FIRE	Location	ICONA Estimation (A)	MVC4-MVC1 (B)[1]	B/A (%)	Aug4 -Jul10 (C)[2]	C/A (%)
A+B	Buñol	21,069	19,800	94	21,600	102
C	Tabernes	1.077	1,300	120	1,400	130
D+E	Carcagente*	667	2,900	434	3,000	450
F	Luchente	3,841	3,600	94	3,600	94
G	Villalonga	1,605	1,400	87	1,900	118

(1) Maximum Value Composites first and fourth

(2) Single images from July 10 and August 4.

(*) See text for explanation

Regarding the differences in performance between single NDVI and MVC images for estimating burned land, for most of the fires single NDVIs show better agreement with official statistics. As we had hypothesized, the effect of slight misregistrations between single scenes tends to create a smoothing effect on the MVC images. As a consequence, the sharp contrast between burned and healthy vegetation is faded and multitemporal differences tend to underestimate the affected area.

4.2. Burned area mapping

Figure 5 shows the burned land maps derived from AVHRR imagery overlaid on the perimeter drawn by GPS techniques and Landsat-TM imagery for the case of the Buñol fire. Again, it can be concluded that the estimation from single NDVI images produces better results than from MVC values. It is interesting to point out that the ICONA fire perimeter included an area which was not burned in Buñol's fire but by a previous fire, at the beginning of July. This area is clearly portrayed in Landsat images, because they discriminate not only burned area but also loss of vegetation between the two images.

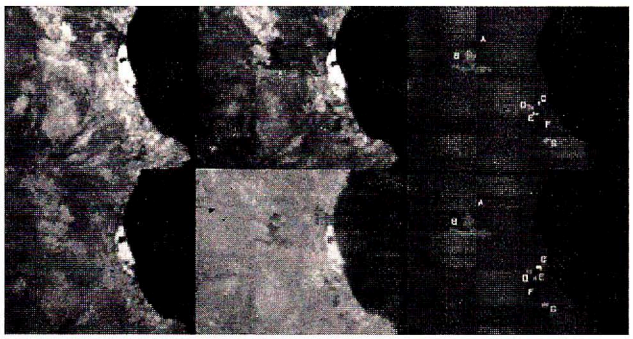

Figure 4 - Fire mapping from decreases in NDVI. In the upper row the MVC images from before and after the fire and the resulting estimation are portrayed. In the lower row single NDVI images from before and after the fire, and the cartography obtained are shown

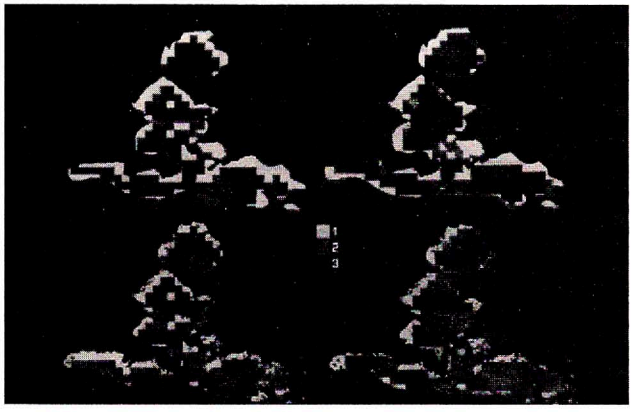

Figure 5 - The two images at the upper row were obtained by overlaying the estimation of burned land from AVHRR imagery using MVC and single NDVI values on the ICONA perimeter, while the ones on the lower row have been obtained by overlaying those estimations on the Landsat-TM derived perimeter

Area evaluation is also more precise with single NDVI than MVC images. Spatial agreement between AVHRR images and fire perimeter (as reported by ICONA) is 68.11 % for single NDVI and 61.55 % for MVC. Both, AVHRR images and fire perimeter show the same spatial pattern, with only minor differences in the borders of the affected area. The relationship with Landsat-TM is also stronger for single NDVI (60.45 %) than for MVC images (55.38 %). In this case, the disagreement between AVHRR and Landsat TM are probably related to the greater sensitivity of the latter to the discrimination of slightly burned vegetation or agricultural bare soils within the fire perimeter, which are not isolated in AVHRR images because of their coarse spatial resolution. However, the agreement between Landsat and NOAA estimations may have been improved if images for the same dates would have been available.

5. CONCLUSIONS

This study has shown that simple techniques for multitemporal change detection of AVHRR NDVI images can be accurately used for burned land estimation, specially in the case of large fires. Single day NDVI values render better estimation than maximum value composites, which tend to be more affected by misregistration. In both cases cloud masking is critical for burned land estimation, as reduction in NDVI values might otherwise be associated with clouds instead of changes in vegetation cover.

Future work will compare these simple change detection techniques with more complex ones, such as principal components, regression analysis or multitemporal classification.

ACKNOWLEDGEMENTS

This project was funded by the Spanish Forest Service (ICONA). Very valuable suggestions were provided by Dr. Ricardo Vélez, the director of the Forest Fire section. Information obtained by the regional center of Valencia was important to assess our results, and specially the report prepared by Mr. Rafael Currás. AURENSA and INFOCARTO, S.A. provided help in reading the AVHRR tapes. Valuable suggestions by the reviewers are also appreciated.

REFERENCES

Abel P., 1990, Prelaunch calibration of the NOAA-11 AVHRR visible and near IR channels: *Remote Sensing of Environment*, **31**: 227-229.

Belward A.S., 1991, Remote sensing for vegetation monitoring on regional and global scales. In: *Remote Sensing and Geographical Information Systems for Resource Management in Developing countries*, (A.S.Belward, and C.R.Valenzuela, editors), Kluwer Academic Publishers, Dordrecht: 169-187.

Cahoon D.R., Stocks B.J., Levine J.S., CoferW.R. & O'Neill K.P. , 1992,. Seasonal distribution of African savanna fires: *Nature*, **359**:812-815.

Che N.& Price J.C., 1992, Survey of Radiometric Calibration Results and Methods for visible and Near Infrared Channels of NOAA-7, -9, and -11 AVHRRs: *Remote Sensing of Environment*, **25**: 19-27.

Chuvieco E. & Congalton R.G., 1988, Mapping and inventory of forest fires from digital processing of TM data: *Geocarto International*, **3**:41-53.

Chuvieco E. & Martín M.P., 1994a, Global fire mapping and fire danger estimation using AVHRR images: Photogrammetric *Engineering and Remote Sensing*, **60**: 563-570.

Chuvieco E. & Martín M.P., 1994b, A simple method for fire growth mapping using AVHRR channel 3 data: *International Journal of Remote Sensing*, **15**: 3141-3146.

ESA, 1992, *SHARP User's Guide*, European Space Agency, Frascati.

Flannigan M.D. & Vonder Haar T.H., 1986, Forest fire monitoring using NOAA satellite AVHRR: *Canadian Journal of Forest Research*, **16**: 975-982.

Herfert M.R. & Lulla K.P., 1990, Mapping continental-scale biomass burning and smoke palls over the Amazon basin as observed from the Space Shuttle: *Photogrammetric Engineering and Remote Sensing*, **56**:1367-1373.

Hirsch S.N., Kruckeberg R.F. & Madden F.H., 1971, The bi-spectral forest detection system. In: Proc. *7th Inter. Symp. on Remote Sensing of Environment*, Ann Arbor: 2253-2259.

Holben B.N., 1986, Characteristics of maximum-value composite images from temporal AVHRR data: *International Journal of Remote Sensing*, **7**: 1417-1434.

Holben B.N., Kaufman Y.J. & Kendall J.D., 1990, NOAA-11 AVHRR visible and near-IR inflight calibration: *International Journal of Remote Sensing*, **11**: 1511-1521.

Kasische E.S., French N.H., Harrell P., Christensen N.L., Ustin S.L. & Barry D., 1993, Monitoring of wildfires in Boreal forest using large area AVHRR NDVI composite image data: *Remote Sensing of Environment*, **45**:61-71.

Kaufman Y.J., Tucker C.J., & Fung I., 1990, Remote sensing of biomass burning in the Tropics: *Journal of Geophysical Research*, **95**:9927-9939.

Langaas S., 1992, Temporal and spatial distribution of savanna fires in Senegal and the Gambia, West Africa, 1989-90, derived from multi-temporal AVHRR night images: *Internationdl Journal of Wildland Fire*, **2**:21-36.

Malingreau J.P., 1984, Remote sensing and disaster monitoring, a review of application in Indonesia. In: *Proc. 18th Intern. Symp.Rem. Sens. of Environment*, Paris: 283-283.

Malingreau J.P., 1990, The contribution of remote sensing to the global monitoring of fires in tropical and subtropical ecosystems. In: *Fire in Tropical Biota*, (J.G.Goldammer, editor), Springer Verlag, Berlin: 337-370.

Matthews A. & Jessell M., 1992, Firescan: a semiautomated system for mapping of bush fires: *6th Australasian Remote Sensing Conference*, Wellington, New Zealand, **2**:166-173.

Milne A.K. & Hall A.M., 1992, Towards the operational detection and mapping of bushfires: *6th Australasian Remote Sensing Conference*, Wellington, New Zealand, **2**:156-165.

Pereira A., Setzer A.W. & Dos Santos J.R., 1991, Fire estimates in savannas of central Brasil with thermal AVHRR/NOAA calibrated by TM/Landsat: *Proc. 24th International Symp. on Remote Sensing of Environment*, Rio de Janeiro: 825-836.

Prins E.M. & Menzel W.P., 1992, Geostationary satellite detection of biomass burning in South America: *International Journal of Remote Sensing*, **13**: 2783-2799.

Robinson J.M., 1991, Fire from space: global fire evaluation using infrared remote sensing: *International Journal of Remote Sensing*, **12**: 3-24.

Setzer A. & Pereira M.C., 1991a, Operational detection of fires in Brazil with NOAA-AVHRR. In: *Proc. 24th. International Symp. on Remote Sensing of Environment*, Rio de Janeiro: 469-482.

Setzer A.W. & Pereira M.C., 1991b, Amazonia biomass burnings in 1987 and an estimate of their tropospheric emissions: *Ambio*, **20**: 19-23.

Tanaka S., Kimura H. & Suga Y., 1983, Preparation of a 1:25.000 Landsat map for assessment of burnt area on Etajima Island: *International Journal of Remote Sensing*, **4**: 17-31.

Watson C.E., Fishman J. & Reitchle H.G.,1990, The significance of biomass burning as a source of carbon monoxide and ozone in the Southern tropics: a satellite analysis: *Journal of Geophysical Research*, **95**:16443-16450.